HHS Public Access

Author manuscript

Nanomedicine (Lond). Author manuscript; available in PMC 2016 August 21.

Published in final edited form as:

Nanomedicine (Lond). 2015 August ; 10(16): 2481–2497. doi:10.2217/NNM.15.90.

Targeting breast cancer with sugar-coated carbon nanotubes

Cale D Fahrenholtz[1], **Mallinath Hadimani**[2], **S Bruce King**[2], **Suzy V Torti**[3], and **Ravi Singh**[*,1,4]

[1]Department of Cancer Biology, Wake Forest University Health Sciences, Hanes Bldg, Rm 4045, Medical Center Blvd, Winston Salem, NC 27157, USA

[2]Department of Chemistry, Wake Forest University, Winston Salem, NC 27109, USA

[3]Department of Molecular Biology & Biophysics, University of Connecticut Health Center, CT 06030, USA

[4]Comprehensive Cancer Center of Wake Forest School of Medicine, Winston Salem, NC 27157, USA

Abstract

Aims—To evaluate the use of glucosamine functionalized multiwalled carbon nanotubes (glyco-MWCNTs) for breast cancer targeting.

Materials & methods—Two types of glucosamine functionalized MWCNTs were developed (covalently linked glucosamine and non-covalently phospholipid-glucosamine coated) and evaluated for their potential to bind and target breast cancer cells *in vitro* and *in vivo*.

Results & conclusion—Binding of glyco-MWCNTs in breast cancer cells is mediated by specific interaction with glucose transporters. Glyco-MWCNTs prepared by non-covalent coating with phospholipid-glucosamine displayed an extended blood circulation time, delayed urinary clearance, low tissue retention and increased breast cancer tumor accumulation *in vivo*. These studies lay the foundation for development of a cancer diagnostic agent based upon glyco-MWCNTs with the potential for superior accuracy over current radiopharmaceuticals.

Keywords

biocompatibility; imaging; metabolism; nanoparticle; self-assembly

Background

Breast (and other) cancers exhibit increased sugar uptake due to alterations in the normal metabolism of glucose [1] and elevated expression of glucose transporters (GLUTs) [2]. Clinically, the use of ^{18}F-fluorodeoxyglucose (^{18}FDG) to identify tumors exhibiting high glucose uptake by positron emission tomography (PET) has had a dramatic impact on breast

[*]Author for correspondence: Tel.: +1 336 713 4434, Fax: +1 336 716 0255, rasingh@wakehealth.edu.

Ethical conduct of research

The authors state that all animal investigations were performed with prior approval and in accordance with the Wake Forest University Institutional Animal Care and Use Committee. The authors state that they have obtained appropriate institutional review board approval or have followed the principles outlined in the Declaration of Helsinki for all human or animal experimental investigations. In addition, for investigations involving human subjects, informed consent has been obtained from the participants involved.

cancer management through improved staging [3]. When injected into a patient's blood stream, ^{18}FDG is taken up and retained by cancer cells at a more rapid rate than normal cells, and tumor sites show up as ‘hot spots’ on a PET scan. Although accuracy in detecting tumors larger than 2 cm is high, ^{18}FDG-PET may miss approximately one third of invasive cancers smaller than 1 cm [4,5]. As early and accurate diagnosis is still the most effective approach to treating breast cancer, improvements in the use of technology to detect and monitor cancer will have a dramatic effect on human health.

Recent developments in the application of nanomaterials such as carbon nanotubes (CNTs) for cancer imaging may allow for significant improvements in detection of disseminated tumors (reviewed in [6]). CNTs consist of sheets of sp^2 carbon rolled into single- or multi-walled tubes and are extremely useful for biomedical applications due to their extraordinary thermal, optical, and electrical properties [7]. They offer many advantages for targeted molecular imaging of cancer; foremost is their ability to deliver large numbers of imaging agents per each targeted molecular recognition event, which can improve the sensitivity and specificity of imaging [8,9]. Secondly, CNTs can be engineered to deliver radiotracers [9–11], MR contrast agents [12] and their innate properties enable ultrasound [13], photoacoustic [14] and near-infrared (NIR) imaging [15]. Thirdly, they are internalized by cells [16,17] and can act as delivery vehicles for therapeutic applications including chemotherapy [18], radiotherapy [8,9] gene delivery [19,20] and as mediators for photothermal cancer therapy [21].

Pristine (pure carbon) CNTs have hydrophobic, low-polarity surfaces, which present challenges for dispersion in physiologic solutions [22]. In order to increase the aqueous dispersion of CNTs, it is necessary to chemically functionalize their surfaces. To this end a variety of strategies including acid oxidation [23], cycloaddition reactions [19] and adsorption of amphiphilic surfactants [24] have been developed to render CNT surfaces more hydrophilic. Further chemical modification and biofunctionalization of these hydrophilic CNTs makes it possible to generate bioactive nanotubes bound to nucleic acids [19,20,25], antibodies [24], peptides [26] and carbohydrates (reviewed in [27]).

The ability to enhance carbohydrate mediated interactions through multivalent display on functionalized nanomaterials has generated significant interest [28]. CNTs are well suited for this application because the high aspect ratio and surface area of CNTs enable the display of a large number of carbohydrates [29–31] in a manner that that favors multivalent ligand–receptor interactions [32–34]. This is of particular importance for studying carbohydrate binding due to the relatively low binding affinity of individual mono- and polysaccharides for their target ligands [28]. Carbohydrate functionalized CNTs have proven effective for biosensing [35], bacterial interaction [36,37] and specific molecular binding/recognition applications in cell-free systems [33,38,39]. For interaction with mammalian cells, functionalization of CNTs with simple sugars provides benefits of high aqueous dispersion stability and low cytotoxicity *in vitro* [39–41] and *in vivo* [41,42]. Functionalization with an appropriate sugar may allow for targeting of the nanotubes to sites of high glucose uptake such as tumors. However, the affinity of carbohydrate functionalized CNTs for binding receptors or transporters expressed by mammalian cells has not been studied extensively.

Currently, FDG is the only sugar used clinically for cancer imaging. Glucosamine (2-amino-2-deoxyglucose), an FDG derivative, also binds to glucose transporters overexpressed by cancer cells and glucosamine derivatives have shown potential as a cancer imaging agent in preclinical studies [43–45]. Several studies have demonstrated that functionalization of nanoparticles with glucosamine or other glucose derivatives can be used as a strategy to increase the cell uptake or alter the biodistribution of the glyconanoparticles as compared with nonglycoparticles [46–50]. However, all previous studies traced the nanoparticle core rather than the displayed sugar. We hypothesized that radiolabeled sugars could be used as both a nanoparticle targeting and detection agent and that multivalent display of the a radiolabeled sugar from a nanoparticle scaffold would lead to increased sugar binding, uptake and signal amplification due to the additive effects resulting from incorporating multiple radiolabels and targeting ligands into a single nanometer-sized particle.

Here we report the development of glycomultiwalled carbon nanotubes (glyco-MWCNTs). Two types of glyco-MWCNTs were evaluated. Glucosamine was covalently conjugated directly to oxidized MWCNTs (MWCNT-GlcN) or to distearyl-phosphotidylcholinepolyethylene glycol (DSPE-PEG-GlcN) which was then used to noncovalently coat oxidized MWCNTs through hydrophobic interactions (MWCNT-DSPE-PEG-GlcN). To delineate the role that GLUTs played in the binding and uptake of the glyco-nanotubes, breast cancer cells were exposed to glyco-MWCNTs alone or in combination with inhibitors of sugar transport (excess glucosamine; cytochalasin B) or cytochalasin D, an actin depolymerizing agent that can inhibit macropinocytosis and caveolin-mediated endocytosis, independent of sugar transport. We also performed *in vivo* studies to evaluate differences in tumor accumulation, blood kinetics, biodistribution and body clearance between free glucosamine, MWCNT-GlcN and MWCNT-DSPE-PEG-GlcN. Our data demonstrate the capacity for breast cancer targeting *in vitro* and *in vivo* through multivalent interactions between glucosamine displayed on MWCNTs and GLUTs expressed on breast cancer cells and suggest glyco-MWCNTs may show promise as a tumor-targeted diagnostic agent.

Materials & methods

Cell culture & chemical reagents

MDA-MB-231 breast cancer cells were obtained from American Type Culture Collection (CRM-HTB-26). MDA-MB-231 were maintained in complete media consisting of DMEM/F12 (Life Technologies) supplemented with 10% fetal bovine serum (Sigma-Aldrich), 100 IU/ml penicillin and 100 μg/ml streptomycin (Life Technologies). D-glucosamine hydrochloride was purchased from Acros Organics. Kaiser test reagents, cytochalasin B, cytochalasin D and 2-(N-morpholino) ethanesulfonic acid solution (MES, 1 M in water) were obtained from Sigma Aldrich. Short acid oxidized MWCNT (0.5–2 μm in length; 8–15 nm diameter) were obtained from Nanostructured & Amorphous Materials Inc. (TX, USA). N-hydroxysuccinimide ester (NHS) of DSPE-PEG(5000) (DSPE-PEG-NHS) was obtained from Nanocs. 1-ethyl-3-(3-dimethylaminopropyl)carboiimide (EDC) and

sulfo-NHS were obtained from Pierce. ^{3}H-glucosamine (specific activity: 37.3 Ci/mmol) was obtained from Perkin Elmer.

Synthesis of glyco-MWCNTs

To reduce size and increase aqueous dispersibility, the initial stock of MWCNTs was further acid oxidized using sulfuric acid and nitric acid treatment (3:1 mixture) for 3 h at 75°C. The MWCNTs were resuspended in sodium hydroxide (1.0 N), sonicated for 10 min, and incubated at room temperature for 30 min to remove carbonaceous debris formed during oxidation. Next, MWCNTs were resuspended in hydrochloric acid (0.1 N), sonicated for 10 min and incubated at room temperature for 30 min to reprotonate the carboxyl groups introduced during the initial acid oxidation. Between each acid or base treatment, the MWCNTs were collected on a 0.1 μm Omnipore JV filter membrane (Millipore) by vacuum filtration and washed extensively with water until the flow thru was clear and the pH was neutral. Finally, the MWCNTs were scraped from the membrane, dried and used for conjugation to glucosamine. A two-step process was used to create radiolabeled ^{3}H-MWCNT-GlcN. First ^{3}H-glucosamine (100 μCi) was reacted with 10 mg of MWCNTs and EDC/sulfo-NHS in 50 mM MES buffer (pH 5.5) overnight in the dark. This was then followed by a second reaction with excess cold glucosamine and fresh EDC/sulfo-NHS in 50 mM MES to increase the glucosamine functionalization of the nanotubes. The final ^{3}H-MWCNT-GlcN were collected on a 0.1 μm Omnipore JV membrane by vacuum filtration and washed extensively with water until radioactivity in the flow thru was undetectable. For the second type of glyco-MWCNTs, 2 mg DSPE-PEG-NHS was reacted with 100 μCi ^{3}H-glucosamine for 1 h in 200 μl PBS (pH 7.4), then added to 1 ml PBS (pH 7.4) containing 10 mg/ml DSPE-PEG-NHS and 0.18 mg/ml glucosamine, and incubated overnight in the dark at 4°C. The following day 10 mg acid-oxidized MWCNTs were added to the DSPE-PEG-GlcN solution, then sonicated six times for 10 min, exchanging water between cycles to prevent overheating as previously described [22]. The MWCNTs and DSPE-PEG-GlcN self-assembled through hydrophobic interactions (MWCNT-DSPE-PEG-GlcN). The progress of all reactions was monitored by the ninhydrin reaction [51] using a Kaiser test kit (Sigma) to demonstrate the formation of a bond between the EDC or NHS activated carboxyl group and the free amine on glucosamine, which is indicated by the a decrease in the amount of free amine. As a final step, glycosylated MWCNTs were washed extensively using a 30 kD size exclusion spin column (Millipore) to remove any small molecules not associated with the nanotubes. Washing was repeated until the concentration of radioactivity in the final filtrate represented less than 5% of the concentration of radioactivity remaining in the fraction containing the glyco-MWCNTs.

Physicochemical characterization

The hydrodynamic diameter of glyco-MWCNTs was assessed by dynamic light scattering (DLS) using a Zetasizer NS90 (Malvern Instruments) in both water and PBS in automatic mode, and by nanoparticle tracking analysis (NTA) using a Nanosight NS500 (Malvern Instruments). The ζ-potential of glyco-MWCNTs was assessed in Milli-Q water at pH 6.8–7 using the Zetasizer NS90. Concentration of glyco-MWCNTs was determined by NTA. Glyco-MWCNTs were diluted 50,000-fold in 0.1 μm filtered milli-Q water in triplicate and at least three measurements of each sample were taken. Additional dilutions were assessed

to ensure linearity of the measurements with changes in concentration. Nanoparticle tracking analysis was used to determine the particle concentration of glyco-MWCNTs. Measurements were made at 25°C using the Nanosight NS500 running NTA v3.0 software with the following settings used for data acquisition: temperature: 25°C; camera level: 16; duration: 90 s; detect threshold: 4. To determine particle concentrations, samples from glyco-MWCNT preparations used for *in vivo* studies were diluted in triplicate (1:5000 and 1:50000) in degassed Milli-Q (Type I) water and concentration and particle size distributions were determined. Three measurements from each dilution were taken.

Cell-uptake assays

Two hundred thousand MDA-MB-231 cells were seeded in 12-well plates (BD Falcon) in 1 ml of complete media and allowed to attach overnight. The following day cells were washed once in PBS and media was replaced with glucose-free DMEM (Life Technologies) for 30 min. Medium was aspirated and replaced with 1 ml of glucose-free DMEM containing ^{3}H-glyco-MWCNTs or the relevant ^{3}H-labeled controls. For competition or uptake inhibition studies, cold glucosamine, cytochalasin B or cytochalasin D were added during both the 30 min pretreatment and at the time of adding radiolabeled materials. For all radiolabeled assays 0.025–0.05 μCi per well were used. Cells were incubated for the times indicated in the figures, washed twice in ice-cold PBS and harvested in cell lysis buffer (20 mM TRIS, 0.1M NaCl, 2% Triton-X, 10 mM EDTA). Cell lysates were transferred to scintillation vials, mixed with scintillation cocktail (Ecolume, MP Biomedicals) and ^{3}H activity was assessed using a scintillation counter (Beckman Coulter LS6500).

Transmission electron microscopy

Six hundred thousand MDA-MB-231 cells per well were plated on six-well dishes in 2 ml of media and allowed to recover for 24 h at 37°C. Cells were washed twice with PBS, then glucose-free DMEM containing glyco-MWCNTs was added and cells were incubated for 60 min. Cells were washed three times with PBS, scraped and then fixed in 4% glutaraldehyde at 4°C overnight. Next, cells were pelleted, embedded in resin, cut into ultrathin sections (80 nm) and placed on copper coated formvar grids then imaged using a Tecnai Spirit transmission electron microscope (FEI).

In vivo biodistribution assays

All animal experiments were performed with prior approval by Wake Forest University Institutional Animal Care and Use Committee. Female, 8–10-week-old *nu/nu* mice were purchased from the National Cancer Institute. Mice were housed in groups of five in individually ventilated cages with a 12 h light/dark cycle and were allowed access to food and water *ad libitum*. Mice were allowed to acclimatize for 2 weeks prior to beginning experiments. For tumor inoculation, MDA-MB-231 cells in Matrigel (BD Biosystems) (50 μl containing 2×10^{6} cells) were injected into the fourth inguinal mammary fat pad of mice. Tumor growth was monitored by calipers and volume was determined using the formula: volume = 0.52 × (width) × (length) × (width + length)/2 where length and width are the two largest perpendicular diameters. When the tumors reached an average volume of 250 mm^{3} (approximately 3 weeks postimplantation), mice were injected intravenously with ^{3}H-

glucosamine, ^{3}H-DSPE-PEG-GlcN, ^{3}H-MWCNT-GlcN, ^{3}H-MWCNT-DSPE-PEG-GlcN, or PBS. Mice were then housed in metabolic cages to allow for collection of urine. Blood (25 μl) was collected from the tail vein at the intervals indicated. Tissue was harvested, weighed and radioactivity in harvested tissue was quantified similarly to previously described methods [11]. Briefly, tissues were dissolved 2 ml Scintigest (Fisher), then placed in a 60°C shaking incubator overnight. Samples were decolorized with hydrogen peroxide and glacial acetic acid was added to reduce chemiluminescence. Samples were topped with scintillation cocktail (Cytoscint ES, MP Biomedicals), shaken vigorously to mix, and radioactivity was measured in a Beckman Coulter LS6500 liquid scintillation counter using default settings for ^{3}H with active correction for sample autoluminescence (Lumex) and color quenching (H-number plus). Readings of each tissue from PBS treated mice were subtracted from the readings obtained from ^{3}H-treated mice to account for and remaining background luminescence.

Results

Physicochemical characterization of glycosylated MWCNTs

Physicochemical factors including particle size, shape, density and surface chemistry are all known to affect internalization of nanoparticles by cells and can alter rates of sedimentation onto a cell monolayer leading to alterations in the apparent uptake rate [52,53]. We therefore prepared two versions of glyco-MWCNTs and evaluated their physicochemical properties and dispersion stability prior to conducting cell binding and uptake assays. Initially, carbodiimide mediated linkage chemistry was employed to covalently conjugate glucosamine to carboxyl groups on acid-oxidized MWCNTs (MWCNT-GlcN). Alternatively, a self-assembly technique was used to noncovalently coat MWCNTs with glucosamine conjugated to distearyl–phosphotidylcholine-polyethylene glycol (DSPE-PEG-GlcN) through hydrophobic interactions (MWCNT-DSPE-PEG-GlcN). Schematics of the two types of glycol-MWCNTs are shown in Figure 1. Notably, prior to conjugation of glucosamine to the MWCNTs, the acid oxidized tubes were washed in sodium hydroxide to remove fulvic acids formed during acid treatment from the surface of the nanotubes to avoid the possibility of functionalizing an adsorbed layer of carbonaceous debris [23].

The hydrodynamic diameter, ζ-potential and particle concentration of MWCNT-GlcN and MWCNT-DSPE-PEG-GlcN were determined by DLS and NTA. In water, all particle preparations were found to possess negative ζ-potentials and exhibit monomodal particle size distributions with a high degree of correlation between the hydrodynamic diameter assessed by DLS as compared with NTA (representative examples are shown in Supplementary Figure 1 [please see online at www.futuremedicine.com/doi/full/10.2217/NNM.15.90] for MWCNT-GlcN and Supplementary Figure 2 for MWCNT-DSPE-PEG-GlcN). As compared with MWCNT-GlcN, MWCNT-DSPE-PEG-GlcN dispersed in water were smaller (109 vs 182 nm by DLS), which may be due to the extensive sonication used to disperse and coat the MWCNTs with DSPE-PEG-GlcN. Electron micrographs also indicate that MWCNT-DSPE-PEG-GlcN are generally smaller than MWCNT-GlcN and show that both types of glyco-MWCNTs are disentangled (Supplementary Figures 1D & 2D). MWCNT-DSPE-PEG-GlcN were less negatively charged than MWCNT-GlcN (−17.6 vs

−38.3), which is expected due to the charge shielding provided by coating MWCNTs with DSPE-PEG-GlcN. When dispersed in PBS, MWCNT-GlcN began to aggregate and sediment over time (Supplementary Figure 3). By contrast, MWCNT-DSPE-PEG-GlcN remained stably suspended in PBS without aggregating for several months. The consequences of these differences will be discussed below in greater detail.

Glyco-MWCNTs exhibit sugar-specific interactions with breast cancer cells

In order to assess the binding and uptake kinetics of the glyco-MWCNTs, MDA-MB-231 breast cancer cells were treated for 0 to 90 min with equivalent radioactive doses (approximately 50 nCi per well) of ^{3}H-MWCNT-GlcN, free ^{3}H-GlcN, ^{3}H-MWCNT-DSPE-PEG-GlcN or free ^{3}H-DSPE-PEG-GlcN. Cells were then washed with PBS and the radioactivity in the cell-associated fraction (which includes both the surface bound and internalized ^{3}H-GlcN or its nanoparticle conjugate) was quantified using a liquid scintillation counter. As shown in Figure 2A, both ^{3}H-MWCNT-GlcN and ^{3}H-MWCNT-DSPE-PEG-GlcN were taken up more rapidly and to a greater extent than free ^{3}H-GlcN. Cell binding/uptake reached a plateau by 60 min and significantly more ^{3}H-MWCNT-GlcN or ^{3}H-MWCNT-DSPE-PEG-GlcN was bound or internalized by the cells than ^{3}H-GlcN (3.4% or 1.9 vs 1.4% of total dose respectively) after 90 min. Notably, free ^{3}H-DSPE-PEG-GlcN was not taken up by cells and remained extracellular for the duration of the experiment. The increased accumulation of ^{3}H-MWCNT-GlcN compared with ^{3}H-MWCNT-DSPE-PEG-GlcN is in part due to aggregation of ^{3}H-MWCNT-GlcN in the media leading to sedimentation. Importantly, the lack of cell associated of ^{3}H-DSPE-PEG-GlcN in the absence of MWCNTs indicated that all cellular accumulation observed was exclusively mediated by the fraction of ^{3}H-DSPE-PEG-GlcN adsorbed onto the MWCNTs. These results demonstrate that glyco-MWCNTs increased the cell associated fraction of the conjugated sugar as compared with the free sugar.

To delineate the role that GLUTs played in the binding and uptake of ^{3}H-MWCNT-GlcN and ^{3}H-MWCNT-DSPE-PEG-GlcN, MDA-MB-231 breast cancer cells were treated with competitive inhibitors of sugar transport. Control experiments using ^{3}H-GlcN were run to demonstrate the activity of the sugar transport inhibitors. Structurally and functionally, each GLUT possesses an exofacial and an endofacial sugar binding domain. Both sites are required for sugar transport across the plasma membrane, but only the exofacial site mediates binding to extracellular sugars [54]. Excess glucosamine was used to compete binding at the exofacial sugar binding site and cytochalasin B, an inhibitor of sugar transport that acts by binding to the endofacial surface of GLUTs, was used to prevent the internalization of extracellular sugars [55].

For the first experiment, cells were pretreated with 10 mM cold glucosamine for 30 min prior to the addition of glyco-MWCNTs to determine if the free sugar could compete for cell binding or uptake. As shown in Figure 2B & C, this concentration was sufficient to significantly reduce the cell associated fraction of ^{3}H-GlcN, ^{3}H-MWCNT-GlcN and ^{3}H-MWCNT-DSPE-PEG-GlcN by greater than 90, 33 and 22%, respectively. For the second experiment, 5 μM cytochalasin B was added to the cells 30 min prior to the addition of the two types of nanotubes to determine to role translocation of the displayed sugar to the

intrafacial binding site played in the cell association of the glycosylated nanotubes. Despite being sufficient to block >90% of the uptake of ^{3}H-GlcN, treatment of MDA-MB-231 cells with 5 μM cytochalasin B had no significant effect on the cellular accumulation of ^{3}H-MWCNT-GlcN and ^{3}H-MWCNT-DSPE-PEG-GlcN. It is important to note that as shown in Figure 2A, free (not absorbed onto MWCNTs) ^{3}H-DSPE-PEG-GlcN was not taken up by MDA-MB-231 cells. Because ^{3}H-DSPE-PEG-GlcN was not taken up by cells, competition studies using this molecule were uninformative and are not shown.

MWCNTs are too large to enter cells via small molecule transporters such as GLUTs, and though glucosamine functionalization increases the accumulation of nanotubes at the cell surface through binding to GLUTs, entry into cells is likely to depend upon other mechanisms. This is consistent with the results of our experiments which indicate that competition at the exofacial sugar binding site of GLUTs, but not at the intrafacial site, reduced the fraction of glyco-MWCNTs found to associate with cells. CNTs are known to translocate across cell membranes using several distinct mechanisms including endocytosis (macropinocytosis, calveolin-mediated, clathrin-dependent), receptor mediated uptake, and through ‘nanoneedle’ effects involving direct piercing of cell membranes [56]. There are limited methods to inhibit each of these uptake mechanisms without having a significant impact on glucose transport as well. However, cytochalasin D, an actin depolymerizing agent, can inhibit macropinocytosis and caveolin-mediated endocytosis with minimal effect on sugar transport. As shown in Figure 3A, treatment of MDA-MB-231 cells with cytochalasin D decreased the cellular accumulation of MWCNT-GlcN by 34% as compared with a nonsignificant 10% reduction of ^{3}H-GlcN transport. Strikingly, under similar conditions, cytochalasin D had no effect on cellular accumulation of MWCNT-DSPE-PEG-GlcN (Figure 3B). These results indicate that macropinocytosis and/or caveolin-mediated endocytosis played a significant role in cellular retention of MWCNT-GlcN, but did not influence the accumulation of MWCNT-DSPE-PEG-GlcN.

As a follow up to these studies, we incubated MDA-MB-231 cells with ^{3}H-MWCNT-GlcN or ^{3}H-MWCNT-DSPE-PEG-GlcN for an hour. Cells were then washed, fixed and processed for imaging by TEM. Electron micrographs show that ^{3}H-MWCNT-GlcN generally were found within intracellular vesicles, often in aggregates (Figure 3C), which is consistent with our DLS data that indicated this type of glyco-MWCNT tended to aggregate in physiologic solution. In contrast, ^{3}H-MWCNT-DSPE-PEG-GlcN were internalized by cells and direct piercing of the cell membrane played a role in uptake, but many of the nanotubes remained localized to the cell surface (Figure 3D). Combined, these results support a model in which specific interactions with GLUTs contribute to the binding of glyco-MWCNTs to cells but not their internalization, which requires non-GLUT mediated uptake mechanisms.

Glyco-MWCNTs increase the delivery of radiolabeled sugars to tumors in mice

An *in vivo* study was conducted to evaluate the effect that conjugation to MWCNTs had on the blood and urinary clearance, biodistribution, and tumor targeting of ^{3}H-GlcN. In an initial study, nude mice were administered a 0.1 μCi dose of ^{3}H-MWCNT-GlcN (approximately $7.3 \pm 0.3 \times 10^{13}$ particles as determined by NTA) by tail vein injection. Because ^{3}H-MWCNT-GlcN aggregated in PBS, a solution of 5% L-glucose in water (weight

to volume) was used to render the delivery vehicle isotonic with blood. Dynamic light scattering indicated that ^{3}H-MWCNT-GlcN did not aggregate in 5% L-glucose (Supplementary Figure 3A). L-glucose was selected instead of the more commonly used D-glucose because unlike D-glucose, L-glucose does not compete with glucosamine for binding to glucose transporters [57]. This eliminates any possible competition occurring between the delivery vehicle and the ^{3}H-MWCNT-GlcN for uptake at the tumor. As a control, mice were injected with 5% L-glucose alone. Immediately following injection, mice were placed in metabolic cages and pooled urine was collected at 1 h postinjection, from 1–24 h postinjection, and from 24–48 h postinjection. Three mice treated with ^{3}H-MWCNT-GlcN were sacrificed at 1 h, 24 h and 48 h postinjection. Blood and tissues (liver, spleen, skin, muscle, kidney, heart and lung) were collected at the time of death. Quantification of ^{3}H was performed by liquid scintillation counting, and data were normalized per unit volume body fluid or unit mass of tissue. ^{3}H-MWCNT-GlcN showed marked lung, liver and spleen accumulation (Figure 4A). Between 1 h and 48 h, radioactivity detected in the lung decreased with a concomitant increase in levels detected in the spleen, possibly indicating a redistribution of ^{3}H-MWCNT-GlcN from the lung to the spleen. It is unknown if this was mediated by movement of phagocytic cells containing ^{3}H-MWCNT-GlcN or by the gradual release of ^{3}H-MWCNT-GlcN aggregates from the lung which then were captured by the spleen. Substantial levels of ^{3}H-MWCNT-GlcN were not found in the blood and radioactivity levels in the urine were low, indicative of rapid clearance from blood circulation and minimal renal excretion (Figure 4B, C). Due to the rapid clearance from the blood and high uptake by the lung, ^{3}H-MWCNT-GlcN were deemed unsuitable for further preclinical evaluation for tumor targeting.

In a second study, MDA-MB-231 cells in matrigel were injected into the 4th inguinal fat pad of nude mice. Tumors were allowed to grow for approximately 3 weeks to average volume of 250 mm^{3}. Two doses, a ‘low dose’ of 0.1 μCi or a ‘high dose’ of 1.3 μCi of ^{3}H-GlcN or ^{3}H-MWCNT-DSPE-PEG-GlcN containing $2.3 \pm 0.3 \times 10^{11}$ or $1.6 \pm 0.2 \times 10^{12}$ particles respectively (as determined by NTA) in PBS, were administered to tumor-bearing mice by tail vein injection (3 to 6 mice per group). Intravenous injection of PBS alone or a 0.1 μCi dose of ^{3}H-DSPE-PEG-GlcN alone served as controls. Immediately following injection, mice from each treatment group were placed in a metabolic cage and pooled urine was collected at 1 h postinjection. The mice were then transferred to a clean metabolic cage and pooled urine was collected from 1 to 24 h postinjection. Blood was collected from the tail vein 10 min, 60 min and 24 h postinjection. Mice were euthanized 24 h postinjection and ^{3}H activity in tissue was quantified as detailed above.

As shown in Figure 5A, ^{3}H-GlcN was cleared rapidly from the blood. Only a negligible amount of ^{3}H-GlcN was detectable 60 min postinjection at the low dose and less than 2% ID ml^{-1} of the high dose remained in the blood at the same time point. In contrast, ^{3}H-MWCNT-DSPE-PEG-GlcN displayed sustained blood residence with 20–22% ID ml^{-1} detectable 60 min postinjection for both doses. In comparison to ^{3}H-GlcN, ^{3}H-DSPE-PEG-GlcN also exhibited extended blood residence, but was cleared more rapidly than ^{3}H-MWCNT-DSPE-PEG-GlcN with less than 3% ID ml^{-1} still detectable at 60 min postinjection. After 24 h, little radioactivity was present in the blood for any treatment or control group.

Analysis of radioactivity in the urine indicated that both ^{3}H-GlcN and ^{3}H-DSPE-PEG-GlcN were rapidly excreted in urine with greater than 300% ID ml^{-1} detected within the small volume of urine (between 100 and 200 μl) collected 1 h after injection (Figure 5B). Substantially less radioactivity was detected in the urine excreted over the next 23 h from these groups of mice, though higher concentrations of ^{3}H-DSPE-PEG-GlcN (50% ID ml^{-1}) as compared with ^{3}H-GlcN (7 or 12% ID ml^{-1} depending upon the administered dose) were detected. Radioactivity detected in the urine of mice 1 h after injection of ^{3}H-MWCNT-DSPE-PEG-GlcN was at least tenfold less than that mice treated with ^{3}H-GlcN or ^{3}H-DSPE-PEG-GlcN. This is consistent with the longer blood residence time, which is expected to correlate with a slower rate of excretion, detected for ^{3}H-MWCNT-DSPE-PEG-GlcN as compared with ^{3}H-GlcN and ^{3}H-DSPE-PEG-GlcN. ^{3}H activity in feces was quantified but accurate measurements were not obtained for all groups due to contamination of ^{3}H from the urine and data are not reported. However, fecal clearance over the first 24 h is expected to be low.

Notable differences existed between the organ and tumor distribution of ^{3}H-MWCNT-DSPE-PEG-GlcN, ^{3}H-GlcN and ^{3}H-DSPE-PEG-GlcN in these mice 24 h after injection (Figure 6A). Both ^{3}H-GlcN and ^{3}H-DSPE-PEG-GlcN were not found at appreciable levels in any of the normal tissues tested. In contrast, radioactivity from ^{3}H-MWCNT-DSPE-PEG-GlcN was detected in the liver and spleen, consistent with uptake or filtration by the mononuclear phagocyte system. Less than 1.5 or 4% ID ml^{-1}, depending on dose, was detected in the lung, which was at least fourfold less than that of ^{3}H-MWCNT-GlcN. Radioactivity from ^{3}H-MWCNT-DSPE-PEG-GlcN was also detected in the kidney, though this may have been en route to the urine. Most importantly, more radioactivity from ^{3}H-MWCNT-DSPE-PEG-GlcN than ^{3}H-GlcN was detected in tumors (threefold more at the low dose and twofold at the high dose) and noradio activity was detected in tumors of mice injected with ^{3}H-DSPE-PEG-GlcN (Figure 6B). Additionally, the tumor to muscle ratio of ^{3}H-MWCNT-DSPE-PEG-GlcN was significantly greater than that of ^{3}H-GlcN at both the low and high doses tested (1.7- and 4.7-fold, respectively) (Figure 6C). Combined, these *in vivo* results indicate that ^{3}H-MWCNT-DSPE-PEG-GlcN exhibits several advantages over the corresponding free sugar with regards to potential for cancer detection.

Discussion

MWCNTs have a large surface area that can be decorated with imaging and targeting moieties to increase tumor accumulation and specificity of the imaging signal [34]. Borrowing from ^{18}FDG-PET imaging, we exploited the fact that many cancers express higher levels of sugar transporters than normal tissues and developed sugar coated MWCNTs to target these cells. We found that compared with ^{3}H-GlcN alone, ^{3}H-MWCNT-DSPE-PEG-GlcN displayed an extended blood circulation time, delayed urinary clearance, low tissue retention and increased breast cancer tumor accumulation *in vivo*. ^{3}H-MWCNT-DSPE-PEG-GlcN also increased the tumor to muscle uptake ratio of the radiolabeled sugar displayed on the nanotube surface in comparison to the free sugar. This is the first study to examine the possibility of using glyconanotubes for tumor targeting and this study lays the foundation for development of a cancer diagnostic agent based upon MWCNTs with the potential for superior accuracy over current radiopharmaceuticals.

Progress toward translating CNTs from merely interesting to clinically useful has been hampered by safety concerns associated with use of CNTs in the body [58]. Despite an extensive body of research showing that appropriate design can ameliorate many unwanted effects of CNTs, there is a continued debate over their toxicity [21]. The *in vivo* fate of CNTs largely is related to the physicochemical properties of the tubes, and even minor structural or chemical changes to particle surfaces significantly alter the biologic fate of nanoparticles [59]. Therefore, our current work builds upon our previous research which showed that carboxylated MWCNTs noncovalently coated with DSPE-PEG were not thrombogenic following intravenous administration in mice [60]. It is also important to differentiate between the confounding results of toxicity tests designed to determine the effect of accidental exposure to CNTs from tests involving intentional exposure to CNTs which have been modified for biomedical applications [61]. For example, toxicity tests involving very long, pristine CNTs similar to raw material used for industrial purposes demonstrate the potential carcinogenicity of CNTs [62], while CNTs functionalized for biomedical applications, such as those used in our study, are not carcinogenic [63].

Comparisons between actively targeted and nontargeted CNTs generally indicate that targeted CNTs are taken up to a greater degree than untargeted tubes by cells expressing an appropriate partner to the targeting ligand (reviewed in [64]). However, investigations to determine the relative binding kinetics of different nanoparticles are complicated because the physical properties that influence cellular interactions of nanoparticles also affect their solution dynamics [53]. Failure to account for potential changes in solution dynamics induced by physicochemical alterations in the CNTs caused by different modifications to CNT surfaces could affect the interpretation of data demonstrating differential cell binding or uptake. A specific example of this possibility is exhibited by our studies. *In vitro* data showed that ^{3}H-MWCNT-GlcN accumulated in breast cancer cells to a higher degree than ^{3}H-MWCNT-DSPE-PEG-GlcN (3.4% exposed dose vs 1.9%, respectively, after 1 h). ^{3}H-MWCNT-GlcN and ^{3}H-MWCNT-DSPE-PEG-GlcN also displayed distinct colloidal properties – notably, despite similar hydrodynamic diameters and ζ-potential in water at pH 5.5, ^{3}H-MWCNT-GlcN lacked colloidal stability in PBS, pH 7.4. Over time ^{3}H-MWCNT-GlcN aggregated and then began to sediment. By contrast, ^{3}H-MWCNT-DSPE-PEG-GlcN remained well dispersed for months even after dilution in PBS, pH 7.4. Because of the increased stability in physiologic solutions, ^{3}H-MWCNT-DSPE-PEG-GlcN did not settle on cells as rapidly as the ^{3}H-MWCNT-GlcN, which may have led to the observation of ^{3}H-MWCNT-GlcN being taken up by cells more rapidly and to a greater degree than ^{3}H-MWCNT-DSPE-PEG-GlcN *in vitro*.

While our study is the first to examine the binding and uptake of glyco-MWCNTs, several studies by others showed that sugar functionalization of spherical lipid or gold nanoparticles increased their uptake by cancer cells in comparison to nonfunctionalized counterparts [46–50]. A recent study by Male and colleagues demonstrated that such interactions may not be specifically related to binding to GLUTs but instead may be due to alterations in physicochemical characteristics that affect the cell uptake of the glycosylated gold nanoparticles [65]. For our studies, it also is unlikely that MWCNTs, due to their size, can pass through GLUTs to enter cells. However, the display of a large number of glucosamine

molecules on the surface of rod-like stuctures like MWCNTs favors multivalent ligand–receptor interactions which may be considerably stronger than the individual binding of single glucosamine molecules to individual transporters [32–34]. Thus, interactions with glucose transporters may impact the accumulation of glyco-MWCNTs by increasing their localization near the cell membrane or increasing the rate at which the nanotubes subsequently enter the cells. In our studies, competition with 10 mM cold glucosamine was sufficient to block the uptake of free ^{3}H-GlcN by greater than 90%. By contrast, this concentration of cold glucosamine caused only a 20–30% decrease in the cellular association of both ^{3}H-MWCNT-GlcN and ^{3}H-MWCNT-DSPE-PEG-GlcN, which may be indicative of a stronger polyvalent interaction between the tubes and the cells as has been observed for other types of targeted nanotubes [28,37]. It is not clear why free ^{3}H-DSPE-PEG-GlcN (not adsorbed on MWCNTs) was not taken up by cells. The basal affinity of individual glucosamine molecules with GLUTs is low with a K_m in the millimolar range [66] and it is possible that a failure to translocate from the external to the internal binding site on glucose transporters due to the presence of the bulky PEG group may further increase the ‘off’ rate. This is consistent with our data showing that cytochalasin B, which competes with glucosamine for binding to the endofacial sugar binding site of GLUTs, has no impact on the binding of ^{3}H-MWCNT-DSPE-PEG-GlcN.

We note that ^{3}H-MWCNT-GlcN and ^{3}H-MWCNT-DSPE-PEG-GlcN accumulated in and on breast cancer cells via distinct mechanisms. ^{3}H-MWCNT-GlcN cellular accumulation was decreased after treatment with cytochalasin D, an actin depolymerizing agent which can inhibit macropinocytosis and caveolin-mediated endocytosis. On the other hand, the cellular accumulation of 3H-MWCNT-DSPE-PEG-GlcN was not impacted by cytochalasin D. These data indicate that ^{3}H-MWCNT-GlcN, in part, rely on endocytosis for intracellular accumulation, while endocytosis does not appear to play a major role for the uptake of ^{3}H-MWCNT-DSPE-PEG-GlcN. Electron micrographs show that ^{3}H-MWCNT-DSPE-PEG-GlcN are internalized by cells and that direct piercing of the cell membrane plays a role, but many of the nanotubes remained localized to the cell surface. Thus, one explanation for the lack of effect of cytochalasin D on ^{3}H-MWCNT-DSPE-PEG-GlcN is that most of the nanotubes were bound to the cell membrane and remained associated with the cell, but were not internalized by endocytosis. These experiments represent one of the first direct comparisons of the binding and uptake of PEGylated and uncoated CNTs, but more detailed investigations will be needed to generalize our findings.

Numerous sugar functionalized nanoparticles have been developed for tumor targeting *in vivo* [41,46,48,67,68], but prior to our study a direct comparison between the biodistribution and tumor uptake of the free sugar versus the nanoparticle conjugate has not been performed. Previous studies evaluating the biodistribution in mice of nanotubes conjugated to glucosamine via thionyl chloride activation of carboxyl groups on nanotubes (similar to our ^{3}H-MWCNT-GlcN) indicated that the nanotubes accumulated in the lungs [69]. Similar results were obtained using nanotubes conjugated to N-acetylglucosamine via cycloaddition reactions [41]. We also find that ^{3}H-MWCNT-GlcN accumulate in the lungs following intravenous injection and are rapidly cleared from the blood stream. However, ^{3}H-MWCNT-DSPE-PEG-GlcN exhibit a longer blood circulation time, delayed urinary clearance, and

accumulate in the tumors at a substantially higher level in comparison to ^{3}H-MWCNT-GlcN, ^{3}H-GlcN, or free ^{3}H-DSPE-PEG-GlcN. In notable contrast to the ^{3}H-DSPE-PEG-GlcN adsorbed onto the MWCNTs, free ^{3}H-DSPE-PEG-GlcN did not accumulate in any tissue, and was cleared from the blood then excreted at high levels in the urine within an hour of injection. It is important to point out that for all of these studies we traced a radiolabeled sugar rather than the nanotubes themselves. Because of the remarkable difference in the biodistribution and body clearance kinetics between free ^{3}H-DSPE-PEG-GlcN and its MWCNT conjugate, we were able to specifically determine the influence of the nanoparticle and phospholipid conjugation on the uptake, biodistribution and clearance of the sugar. At this point, our studies do not differentiate between detecting the intact sugar or any potential metabolite or degradation product, and pharmacodynamics studies will be necessary to determine if any such derivatives are generated. Furthermore, the long term fate and clearance of the MWCNTs themselves is unknown and requires further investigation.

Conclusion

Nanoparticles designed to recognize and bind tumor cell receptors have shown a great deal of promise in preclinical studies when used to assess the availability of therapeutic targets and monitor the efficacy of treatment [70]. However, for clinical utility in diagnostic imaging of cancer, nanoparticles ideally should be targeted to a biomarker that is universally present. As a step toward this goal, we have developed glyco-MWCNTs that bind to GLUTs which are frequently overexpressed by tumors. We demonstrated the capacity for breast cancer targeting through multivalent interactions between the displayed sugars and GLUTs expressed on breast cancer cells. A basic design was identified for glucosamine functionalized MWCNT exhibiting increased blood circulation, delayed excretion, greater tumor accumulation and improved signal to noise ratio for tumor detection compared with free glucosamine. In the future, our glyco-MWCNT platform will be adapted to display sugars with higher affinity for GLUTs or modified with isotopes suitable for PET imaging. The differential *in vivo* kinetics between free DSPE-PEG-GlcN and the nanoparticle conjugate many facilitate the rapid preparation and labeling of such particles since separation of the components may not be necessary prior to administration. With further development, this new nanomaterial may prove superior to current imaging agents for early-stage cancer detection, and it is anticipated that this agent will serve as the basis for a multimodal platform for future combined cancer therapy and diagnostic applications.

Future perspective

There remains significant room for improvement over the conventional FDG-based PET imaging for cancer detection and staging. CNTs have the ability to display a large number of positron emitters per particle and if properly targeted will improve the signal to noise ratio thus increasing the sensitivity of detecting small metastases that are presently missed. Antibodies, aptamers or other bulky targeting moieties are expensive to produce and may hamper the ability of CNTs to penetrate within tumors. Therefore, small molecular ligands such as the sugars used in our study may overcome these obstacles. Furthermore, the overexpression of GLUTs by many tumor types makes this approach highly versatile for the detection of many types of cancer. At the doses required for imaging, CNTs are expected to

be nontoxic and represent a logical progression in radiopharmaceuticals. We believe that initial studies using low doses of CNTs will pave the way for their use not only as a diagnostic agent, but also as a combination therapeutic delivery system (theranostic). We anticipate that targeted nanomaterials will be further investigated and utilized as a carrier for a personalized theranostic system that is tailored to individual patients/tumors. Personalized medicine using chemotherapeutic-loaded CNTs functionalized with targeting moieties has the potential to simultaneously diagnose cancer, monitor tumor progression, and also monitor efficiency of chemotherapeutic delivery to greatly improve upon current standard of care therapy for breast cancer.

Supplementary Material

Refer to Web version on PubMed Central for supplementary material.

Acknowledgements

The authors are grateful for the support of Ken Grant, Paula Graham and Brandi Bickford of the Wake Forest University Comprehensive Cancer Center (WFUCCC) Cellular Imaging Shared Resource, Yelena Karpova of the WFUCCC Cell and Viral Vector Core Laboratory, and the WFUCCC Synthetic Chemistry Core Lab. The authors thank Brian Bernish, Brittany Eldridge and Jessica Swanner (Wake Forest University Health Sciences) for assistance with data collection and analysis.

Financial and competing interests disclosure

This work was supported in part by grant NCI R00CA154006 (R Singh), NCI R01CA12842 (SV Torti), ARRA supplement R01CA128428-02S1 (SV Torti) and by start-up funds from the Wake Forest School of Medicine Department of Cancer Biology. CD Fahrenholtz was supported by training grant NCI T32CA079448. All shared services were supported by grant NCI CCSG P30CA012197. The authors have no other relevant affiliations or financial involvement with any organization or entity with a financial interest in or financial conflict with the subject matter or materials discussed in the manuscript apart from those disclosed.

No writing assistance was utilized in the production of this manuscript.

References

Papers of special note have been highlighted as:

• of interest; •• of considerable interest

1. Vander Heiden MG, Cantley LC, Thompson CB. Understanding the warburg effect: the metabolic requirements of cell proliferation. Science. 2009; 324(5930):1029–1033. [PubMed: 19460998]
2. Brown RS, Wahl RL. Overexpression of glut-1 glucose transporter in human breast cancer. An immunohistochemical study. Cancer. 1993; 72(10):2979–2985. [PubMed: 8221565]
3. Rosen EL, Eubank WB, Mankoff DA. FDG PET, PET/CT, and breast cancer imaging. Radiographics. 2007; 27(Suppl. 1):S215–S229. [PubMed: 18180228]
4. Schoder H, Gonen M. Screening for cancer with PET and PET/CT: potential and limitations. J. Nucl. Med. 2007; 48(Suppl. 1):4S–18S. [PubMed: 17204716]
5. Ide M. Cancer screening with FDG-PET. Q. J. Nucl. Med. Mol. Imaging. 2006; 50(1):23–27. [PubMed: 16557201]
6. Toy R, Bauer L, Hoimes C, Ghaghada KB, Karathanasis E. Targeted nanotechnology for cancer imaging. Adv. Drug Deliv. Rev. 2014; 76:79–97. [PubMed: 25116445]
7. Kostarelos K, Bianco A, Prato M. Promises, facts and challenges for carbon nanotubes in imaging and therapeutics. Nat. Nanotechnol. 2009; 4(10):627–633. [PubMed: 19809452]
8. Ruggiero A, Villa CH, Holland JP, et al. Imaging and treating tumor vasculature with targeted radiolabeled carbon nanotubes. Int. J. Nanomedicine. 2010; 5:783–802. [PubMed: 21042424]

9. Mcdevitt MR, Chattopadhyay D, Kappel BJ, et al. Tumor targeting with antibody-functionalized, radiolabeled carbon nanotubes. J. Nucl. Med. 2007; 48(7):1180–1189. [PubMed: 17607040]
10. Lacerda L, Soundararajan A, Singh R, et al. Dynamic imaging of functionalized multi-walled carbon nanotube systemic circulation and urinary excretion. Adv. Mater. 2008; 20(2):225–230.
11. Singh R, Pantarotto D, Lacerda L, et al. Tissue biodistribution and blood clearance rates of intravenously administered carbon nanotube radiotracers. Proc. Natl Acad. Sci. USA. 2006; 103(9):3357–3362. [PubMed: 16492781]
12. Ding XF, Singh R, Burke A, et al. Development of iron-containing multiwalled carbon nanotubes for MR-guided laser-induced thermotherapy. Nanomedicine. 2011; 6(8):1341–1352. [PubMed: 21506687]
13. Delogu LG, Vidili G, Venturelli E, et al. Functionalized multiwalled carbon nanotubes as ultrasound contrast agents. Proc. Natl Acad. Sci. USA. 2012; 109(41):16612–16617. [PubMed: 23012426]
14. Chen SL, Chang YC, Zhang C, et al. Efficient real-time detection of terahertz pulse radiation based on photoacoustic conversion by carbon nanotube nanocomposite. Nat. Photon. 2014; 8(7):537–542.
15. Welsher K, Sherlock SP, Dai HJ. Deep-tissue anatomical imaging of mice using carbon nanotube fluorophores in the second near-infrared window. Proc. Natl Acad. Sci. USA. 2011; 108(22): 8943–8948. [PubMed: 21576494]
16. Lacerda L, Raffa S, Prato M, Bianco A, Kostarelos K. Cell-penetrating cnts for delivery of therapeutics. Nano Today. 2007; 2(6):38–43.
17. Raffa V, Ciofani G, Nitodas S, et al. Can the properties of carbon nanotubes influence their internalization by living cells? Carbon. 2008; 46(12):1600–1610.
18. Liu Z, Chen K, Davis C, et al. Drug delivery with carbon nanotubes for *in vivo* cancer treatment. Cancer Res. 2008; 68(16):6652–6660. [PubMed: 18701489]
19. Pantarotto D, Singh R, Mccarthy D, et al. Functionalized carbon nanotubes for plasmid DNA gene delivery. Angew. Chem. Int. Ed. Engl. 2004; 43(39):5242–5246. [PubMed: 15455428]
20. Singh R, Pantarotto D, Mccarthy D, et al. Binding and condensation of plasmid DNA onto functionalized carbon nanotubes: toward the construction of nanotube-based gene delivery vectors. J. Am. Chem. Soc. 2005; 127(12):4388–4396. [PubMed: 15783221]
21. Singh R, Torti SV. Carbon nanotubes in hyperthermia therapy. Adv. Drug Deliv. Rev. 2013; 65(15):2045–2060. [PubMed: 23933617]
22. Liu Z, Tabakman SM, Chen Z, Dai H. Preparation of carbon nanotube bioconjugates for biomedical applications. Nat. Protoc. 2009; 4(9):1372–1382. [PubMed: 19730421]
23. Aviles F, Cauich-Rodriguez JV, Moo-Tah L, May-Pat A, Vargas-Coronado R. Evaluation of mild acid oxidation treatments for mwcnt functionalization. Carbon. 2009; 47(13):2970–2975.
24. Welsher K, Liu Z, Daranciang D, Dai H. Selective probing and imaging of cells with single walled carbon nanotubes as near-infrared fluorescent molecules. Nano Lett. 2008; 8(2):586–590. [PubMed: 18197719]
25. Kam NWS, O'Connell M, Wisdom JA, Dai HJ. Carbon nanotubes as multifunctional biological transporters and near-infrared agents for selective cancer cell destruction. Proc. Natl Acad. Sci. USA. 2005; 102(33):11600–11605. [PubMed: 16087878]
26. Pantarotto D, Partidos CD, Graff R, et al. Synthesis, structural characterization, and immunological properties of carbon nanotubes functionalized with peptides. J. Am. Chem. Soc. 2003; 125(20): 6160–6164. [PubMed: 12785847]
27. Chen YA, Star A, Vidal S. Sweet carbon nanostructures: Carbohydrate conjugates with carbon nanotubes and graphene and their applications. Chem. Soc. Rev. 2013; 42(11):4532–4542. [PubMed: 23247183]
28. Wang X, Ramstrom O, Yan MD. Glyconanomaterials: synthesis, characterization, and ligand presentation. Adv. Mater. 2010; 22(17):1946–1953. [PubMed: 20301131]
29. Chen X, Tam UC, Czlapinski JL, et al. Interfacing carbon nanotubes with living cells. J. Am. Chem. Soc. 2006; 128(19):6292–6293. [PubMed: 16683774]

30. Assali M, Leal MP, Fernandez I, Romero-Gomez P, Baati R, Khiar N. Improved non-covalent biofunctionalization of multi-walled carbon nanotubes using carbohydrate amphiphiles with a butterfly-like polyaromatic tail. Nano Res. 2010; 3(11):764–778.

31•. Gu LR, Lin Y, Qu LW, Sun YP. Carbon nanotubes as a scaffold to display paired sugars in solution. Biomacromolecules. 2006; 7(1):400–402. [PubMed: 16398542] [Developed methods to display simple sugars on the surface of carbon nantotubes, alluding to cell adhesion capabilities.]

32. Mulvey JJ, Villa CH, Mcdevitt MR, Escorcia FE, Casey E, Scheinberg DA. Self-assembly of carbon nanotubes and antibodies on tumours for targeted amplified delivery. Nat. Nanotechnol. 2013; 8(10):763–771. [PubMed: 24077028]

33. Assali M, Leal MP, Fernandez I, Baati R, Mioskowski C, Khiar N. Non-covalent functionalization of carbon nanotubes with glycolipids: glyconanomaterials with specific lectin-affinity. Soft Matter. 2009; 5(5):948–950.

34. Liu Z, Cai WB, He LN, et al. In vivo biodistribution and highly efficient tumour targeting of carbon nanotubes in mice. Nat. Nanotechnol. 2007; 2(1):47–52. [PubMed: 18654207]

35. Sudibya HG, Ma JM, Dong XC, et al. Interfacing glycosylated carbon-nanotube-network devices with living cells to detect dynamic secretion of biomolecules. Angew. Chem. Int. Ed. Engl. 2009; 48(15):2723–2726. [PubMed: 19263455]

36. Gu LR, Elkin T, Jiang XP, et al. Single-walled carbon nanotubes displaying multivalent ligands for capturing pathogens. Chem. Commun. 2005; (7):874–876.

37. Wang HF, Gu LR, Lin Y, et al. Unique aggregation of anthrax (*Bacillus anthracis*) spores by sugar-coated single-walled carbon nanotubes. J. Am. Chem. Soc. 2006; 128(41):13364–13365. [PubMed: 17031942]

38. Khiar N, Leal MP, Baati R, et al. Tailoring carbon nanotube surfaces with glyconanorings: new bionanomaterials with specific lectin affinity. Chem. Commun. 2009; (27):4121–4123.

39. Fu Q, Wu MH, Jiao Z, Wang DQ. Rapid glycosylated functionalization of single-walled carbon nanotubes for lectin recognition. Chem. J. Chinese Universities-Chinese. 2009; 30(3):525–529.

40. Gu LR, Luo PJG, Wang HF, et al. Single-walled carbon nanotube as a unique scaffold for the multivalent display of sugars. Biomacromolecules. 2008; 9(9):2408–2418. [PubMed: 18712920]

41••. Hong SY, Tobias G, Al-Jamal KT, et al. Filled and glycosylated carbon nanotubes for *in vivo* radioemitter localization and imaging. Nat. Mater. 2010; 9(6):485–490. [PubMed: 20473287] [Use of N-acetylglucosamine-functionalized single-walled nanotube showing evidence for development of organ-specific imaging agents *in vivo*.]

42. Pompeo F, Resasco DE. Water solubilization of single-walled carbon nanotubes by functionalization with glucosamine. Nano Lett. 2002; 2(4):369–373.

43. Carroll L, Witney TH, Aboagye EO. Design and synthesis of novel F-^{18}-radiolabelled glucosamine derivatives for cancer imaging. Medchemcomm. 2013; 4(4):653–656.

44. Korotcov AV, Ye Y, Chen Y, et al. Glucosamine-linked near-infrared fluorescent probes for imaging of solid tumor xenografts. Mol. Imaging Biol. 2012; 14(4):443–451. [PubMed: 21971932]

45. Yang DJ, Kim CG, Schechter NR, et al. Imaging with TC-99m ECDG targeted at the multifunctional glucose transport system: feasibility study with rodents. Radiology. 2003; 226(2): 465–473. [PubMed: 12563141]

46•. Chen J, Chen HY, Cui SS, et al. Glucosamine derivative modified nanostructured lipid carriers for targeted tumor delivery. J. Mater. Chem. 2012; 22(12):5770–5783. [Demonstrates use of multivalent display of glucosamine as a targeting moieity for nanoparticles. In this case, nanostructured lipid carriers were employed.]

47. Feng G, Kong B, Xing J, Chen J. Enhancing multimodality functional and molecular imaging using glucose-coated gold nanoparticles. Clin. Radiol. 2014; 69(11):1105–1111. [PubMed: 25023059]

48. Geng F, Xing JZ, Chen J, et al. PEGylated glucose gold nanoparticles for improved in-vivo bio-distribution and enhanced radiotherapy on cervical cancer. J. Biomed. Nanotechnol. 2014; 10(7): 1205–1216. [PubMed: 24804541]

49. Wang C, Jiang Y, Li X, Hu L. Thioglucose-bound gold nanoparticles increase the radiosensitivity of a triple-negative breast cancer cell line (MDA-MB-231). Breast Cancer. 2013

50. Roa W, Xiong Y, Chen J, et al. Pharmacokinetic and toxicological evaluation of multi-functional thiol-6-fluoro-6-deoxy-d-glucose gold nanoparticles *in vivo*. Nanotechnology. 2012; 23(37): 375101. [PubMed: 22922305]
51. Sarin VK, Kent SB, Tam JP, Merrifield RB. Quantitative monitoring of solid-phase peptide synthesis by the ninhydrin reaction. Anal. Biochem. 1981; 117(1):147–157. [PubMed: 7316187]
52. Van Dongen MA, Dougherty CA, Banaszak Holl MM. Multivalent polymers for drug delivery and imaging: the challenges of conjugation. Biomacromolecules. 2014; 15(9):3215–3234. [PubMed: 25120091]
53. Teeguarden JG, Hinderliter PM, Orr G, Thrall BD, Pounds JG. Particokinetics *in vitro*: dosimetry considerations for *in vitro* nanoparticle toxicity assessments. Toxicol. Sci. 2007; 95(2):300–312. [PubMed: 17098817]
54. Cunningham P, Afzal-Ahmed I, Naftalin RJ. Docking studies show that d-glucose and quercetin slide through the transporter glut1. J. Biol. Chem. 2006; 281(9):5797–5803. [PubMed: 16407180]
55. Basketter DA, Widdas WF. Asymmetry of hexose transfer system in human erythrocytes – comparison of effects of cytochalasin b, phloretin and maltose as competitive inhibitors. J. Physiol. (Lond.). 1978; 278:389–401. [PubMed: 671319]
56. Klumpp C, Kostarelos K, Prato M, Bianco A. Functionalized carbon nanotubes as emerging nanovectors for the delivery of therapeutics. Biochim. Biophys. Acta. 2006; 1758(3):404–412. [PubMed: 16307724]
57. Burant CF, Bell GI. Mammalian facilitative glucose transporters: evidence for similar substrate recognition sites in functionally monomeric proteins. Biochemistry. 1992; 31(42):10414–10420. [PubMed: 1420159]
58. Saito N, Haniu H, Usui Y, et al. Safe clinical use of carbon nanotubes as innovative biomaterials. Chem. Rev. 2014; 114(11):6040–6079. [PubMed: 24720563]
59. Li SD, Huang L. Pharmacokinetics and biodistribution of nanoparticles. Mol. Pharmaceut. 2008; 5(4):496–504.
60. Burke AR, Singh RN, Carroll DL, et al. Determinants of the thrombogenic potential of multiwalled carbon nanotubes. Biomaterials. 2011; 32(26):5970–5978. [PubMed: 21663954]
61. Heister E, Brunner EW, Dieckmann GR, Jurewicz I, Dalton AB. Are carbon nanotubes a natural solution? Applications in biology and medicine. ACS Appl. Mater. Interfaces. 2013; 5(6):1870–1891. [PubMed: 23427832]
62. Poland CA, Duffin R, Kinloch I, et al. Carbon nanotubes introduced into the abdominal cavity of mice show asbestos-like pathogenicity in a pilot study. Nat. Nanotechnol. 2008; 3(7):423–428. [PubMed: 18654567]
63. Takanashi S, Hara K, Aoki K, et al. Carcinogenicity evaluation for the application of carbon nanotubes as biomaterials in rash2 mice. Sci. Rep. 2012; 2:498. [PubMed: 22787556]
64. Bertrand N, Wu J, Xu XY, Kamaly N, Farokhzad OC. Cancer nanotechnology: the impact of passive and active targeting in the era of modern cancer biology. Adv. Drug Deliv. Rev. 2014; 66:2–25. [PubMed: 24270007]
65. Gromnicova R, Davies HA, Sreekanthreddy P, et al. Glucose-coated gold nanoparticles transfer across human brain endothelium and enter astrocytes *in vitro*. PLoS ONE. 2013; 8(12):e81043. [PubMed: 24339894]
66. Uldry M, Ibberson M, Hosokawa M, Thorens B. Glut2 is a high affinity glucosamine transporter. FEBS Lett. 2002; 524(1–3):199–203. [PubMed: 12135767]
67. Jiang XY, Xin HL, Gu JJ, et al. Enhanced antitumor efficacy by d-glucosamine-functionalized and paclitaxel-loaded poly(ethylene glycol)-co-poly(trimethylene carbonate) polymer nanoparticles. J. Pharmaceut. Sci. 2014; 103(5):1487–1496.
68. Mehravi B, Ahmadi M, Amanlou M, Mostaar A, Ardestani MS, Ghalandarlaki N. Conjugation of glucosamine with Gd^{3+}-based nanoporous silica using a heterobifunctional ANB-NOS crosslinker for imaging of cancer cells. Int. J. Nanomedicine. 2013; 8:3383–3394. [PubMed: 24101868]
69. Guo JX, Zhang X, Li QN, Li WX. Biodistribution of functionalized multiwall carbon nanotubes in mice. Nucl. Med. Biol. 2007; 34(5):579–583. [PubMed: 17591558]
70. Chapman S, Dobrovolskaia M, Farahani K, et al. Nanoparticles for cancer imaging: the good, the bad, and the promise. Nano Today. 2013; 8(5):454–460. [PubMed: 25419228]

Executive summary

Current status of breast cancer imaging

- Fluorodeoxyglucose positron emission tomography is currently used for breast cancer imaging as standard-care diagnosis; however, a significant portion of small metastatic tumors are missed and methods must be improved.

Development of a glucosamine functionalized carbon nanotube-based imaging agent

- Breast cancers rely on aerobic glycolysis for energy and express higher levels of glucose transporters than normal breast tissues.
- We developed two iterations of glucosamine functionalized multiwalled carbon nanotubes (MWCNT-GlcN [covalently functionalized]; MWCNT-DSPE-PEG-GlcN [noncovalent hydrophobic functionalization]) to target breast cancer through interaction with glucose transporters.

Key results of findings

- Glyco-MWCNTs accumulated in breast cancer cells *in vitro* with altered kinetics compared with free glucosamine.
- Glyco-MWCNTS specifically interacted with glucose transporters noted by competition with free glucosamine.
- MWCNT-DSPE-PEG-GlcN were well tolerated in mice and showed accumulation in breast cancer xenografts.
- MWCNT-DSPE-PEG-GlcN, compared with free glucosamine, displayed an extended blood circulation time, delayed urinary clearance, low tissue retention and increased breast cancer tumor accumulation with an improved signal-to-noise ratio.

Implications

- These studies lay the foundation for the development of breast cancer diagnostic agent based upon glyco-MWCNTs with the potential for superior accuracy over current radiopharmaceuticals and for use in multimodal therapeutic applications.

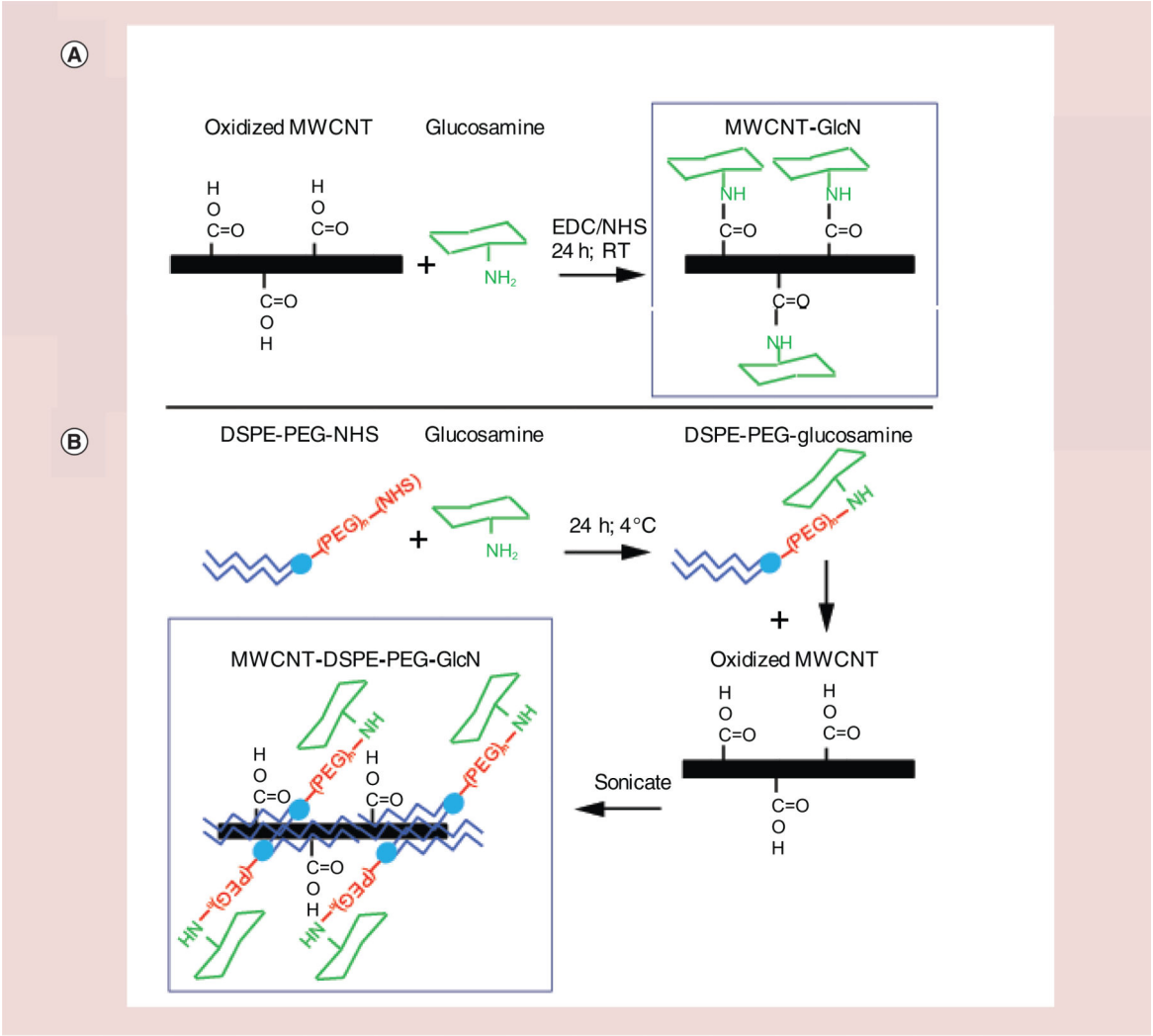

Figure 1. Schematic for glucosamine functionalization of multiwalled carbon nanotubes

Preparation of glyco-MWCNTs is described in detail in 'Materials & methods' and schematically for **(A)** ^{3}H-MWCNT-GlcN and **(B)** ^{3}H-MWCNT-DSPE-PEG-GlcN. GlcN: Glucosamine; MWCNT: Multiwalled carbon nanotube.

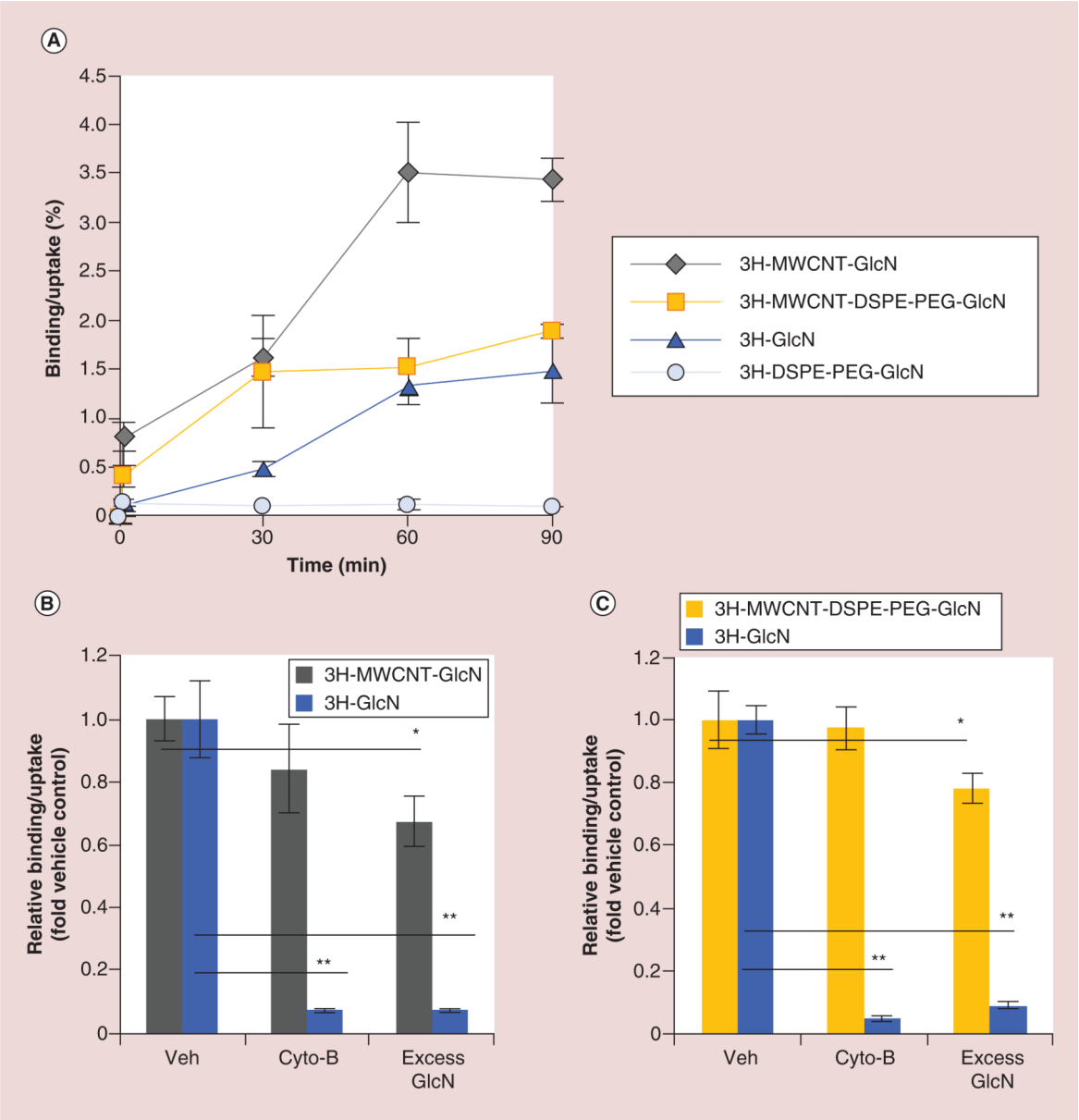

Figure 2. Binding and uptake of glyco-multiwalled carbon nanotubes *in vitro*

To determine binding and uptake rates of glyco-nanotubes by breast cancer cells, **(A)** MDA-MB-231 cells were exposed to ^{3}H-MWCNT-GlcN or ^{3}H-GlcN or ^{3}H-MWCNT-DSPE-PEG-GlcN or free ^{3}H-DSPE-PEG-GlcN in glucose-free media. At the indicated times, cell were washed, lysed, and then radioactivity in the lysate was quantified by scintillation counting. MDA-MB-231 cells were pretreated for 30 min in glucose-free medium containing cytochalasin B (5 μM), excess glucosamine (10 mM) or vehicle, then treated for 60 min with **(B)** ^{3}H-MWCNT-GlcN or control ^{3}H-GlcN or **(C)** ^{3}H-MWCNT-DSPE-PEG-GlcN or control ^{3}H-GlcN in fresh glucose-free media containing cytochalasin B, 10 mM glucosamine, or vehicle as indicated. Sixty minutes later, cell were washed, lysed, and then radioactivity in the lysate was quantified by scintillation counting. Data in **(A)** are displayed as percentage uptake ± standard deviation. Data in **(B & C)** are shown as relative uptake in

the presence of competitor as compared with uptake in the absence of competitor ± standard deviation. All panels are representative of three independent experiments performed in triplicate. (*$p < 0.05$; **$p < 0.01$, two-tailed Student's *t*-test for the indicated pairwise comparisons).

GlcN: Glucosamine; MWCNT: Multiwalled carbon nanotube.

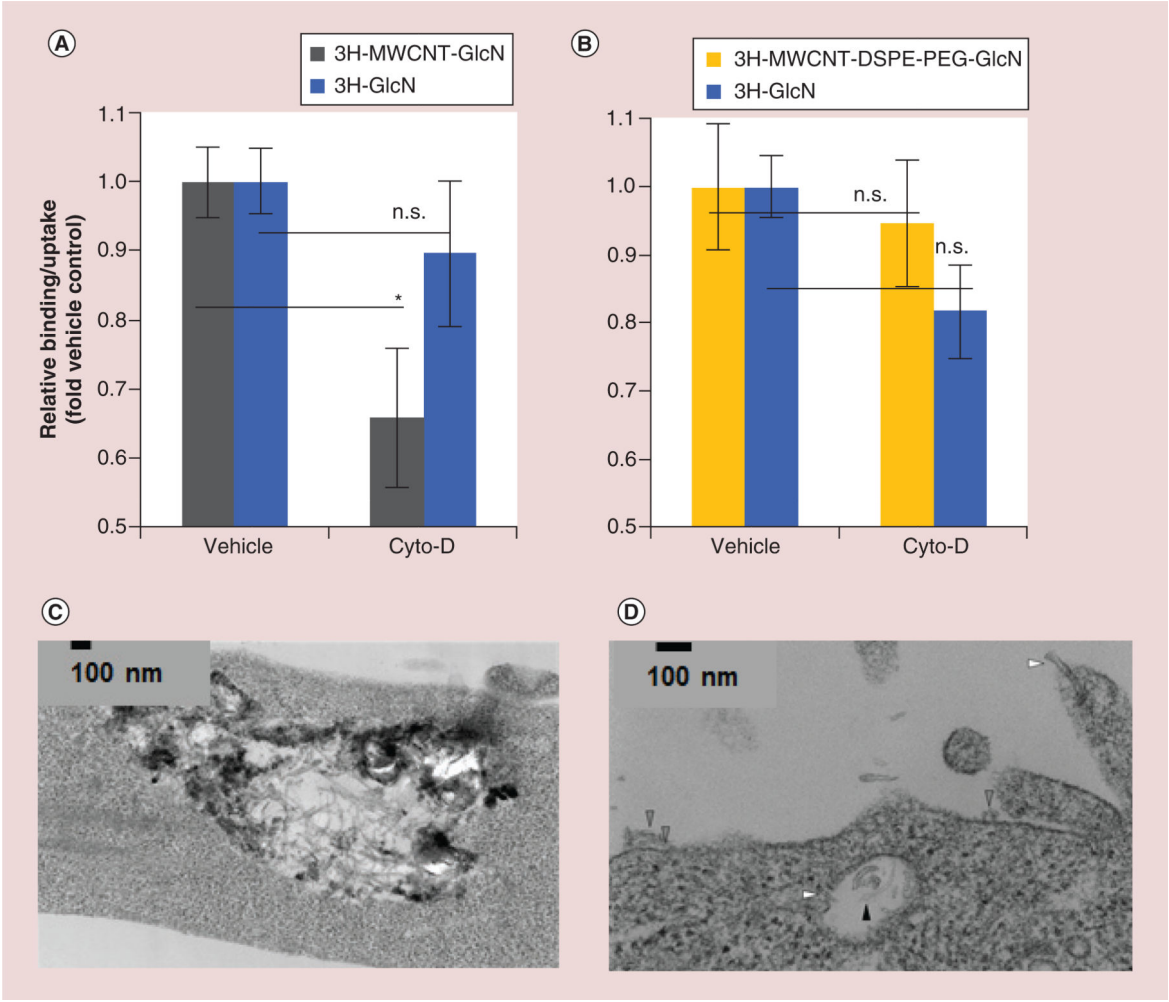

Figure 3. Determination of the mechanism of internalization of glyco-multiwalled carbon nanotubes *in vitro*

To determine the role of endocytosis in the uptake of glyco-MWCNTs, MDA-MB-231 cells were pretreated for 30 min in glucose-free medium containing endocytosis inhibitor cytochalasin D (10 μM) or vehicle, then exposed to **(A)** ^{3}H-MWCNT-GlcN or ^{3}H-GlcN or **(B)** ^{3}H-MWCNT-DSPE-PEG-GlcN or ^{3}H-GlcN in fresh glucose-free media containing cytochalasin D or vehicle. Sixty minutes later, cell were washed, lysed, and then radioactivity in the lysate was quantified by scintillation counting. To determine the subcellular localization of glycosylated MWCNTs, MDA-MB-231 cells were incubated with MWCNT-GlcN or MWCNT-DSPE-PEG-GlcN for 60 min. Cells were washed extensively in PBS, fixed, scraped and then ultrathin sections (80 nm) supported on copper coated formar grids were prepared and imaged by electron microscopy. **(C)** MWCNT-GlcN generally were found in vesicles while **(D)** MWCNT-DSPE-PEG-GlcN are found to be associated with the cell membrane (gray arrows), piecing extracellular and intracellular membranes (white arrows), and entrapped in intracellular vesicles (black arrows). Data in **(A & B)** are shown as relative uptake in the presence of inhibitor as compared with uptake in the absence of inhibitor ± standard deviation and are representative of three independent

experiments performed in triplicate. (*$p < 0.05$, two-tailed Student's *t*-test for the indicated pairwise comparisons).

GlcN: Glucosamine; MWCNT: Multiwalled carbon nanotube; n.s.: Not significant.

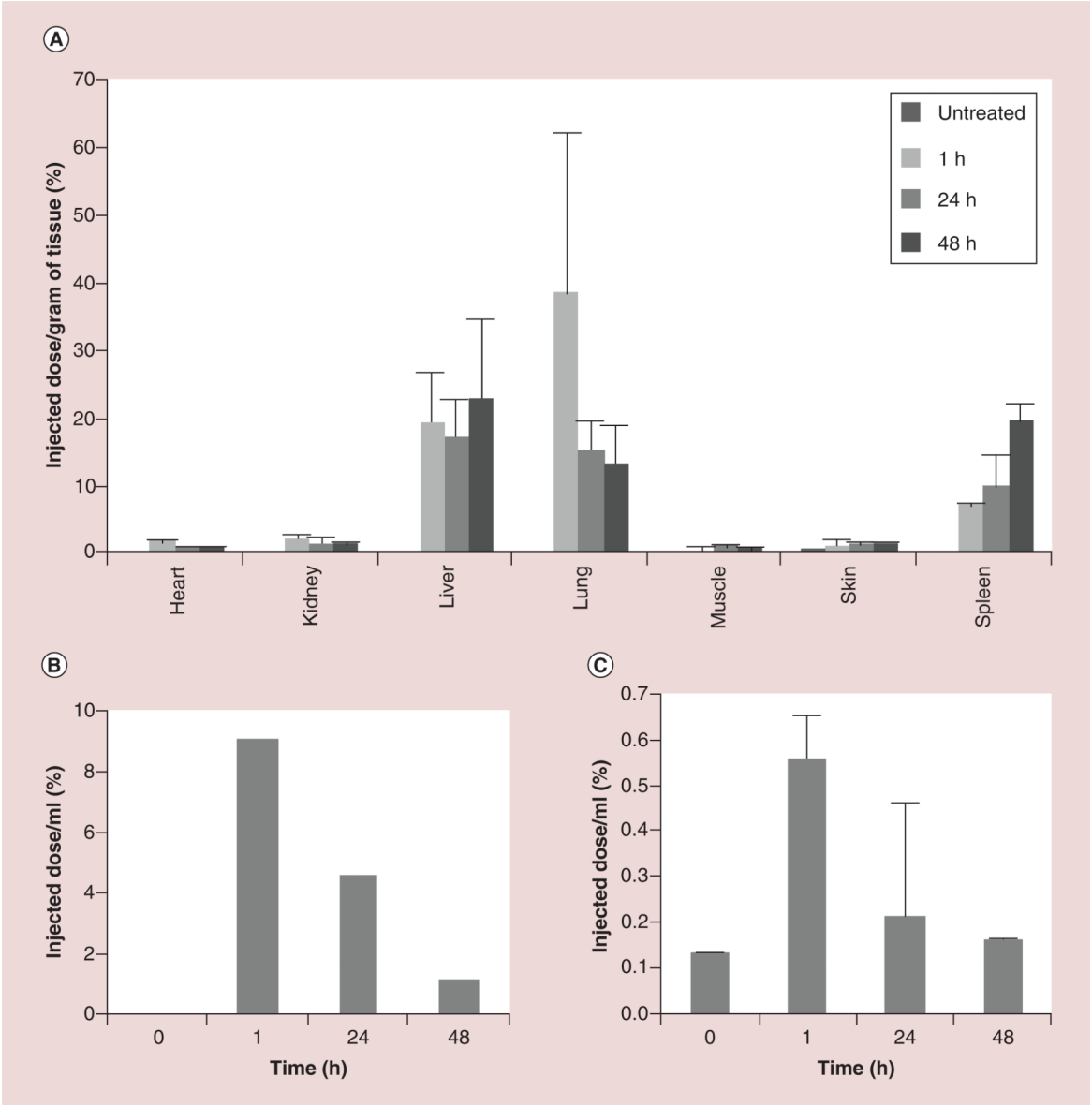

Figure 4. Biodistribution, blood and urinary clearance of ^{3}H-multiwalled carbon nanotube-glucosamine

Nude mice (n = 3 per group) were injected intravenously with 0.1 μCi of ^{3}H-multiwalled carbon nanotube-glucosamine. **(A)** One, 24 and 48 h after injection, tissues were excised, lysed and then radioactivity in the lysate was quantified by scintillation counting. Data are displayed as percentage injected dose per gram tissue ± standard deviation. **(B)** Pooled urine was collected between 0–1 h, 1–24 h and 24–48 h after injection, and assessed by scintillation. **(C)** Blood samples were drawn 0, 1, 24 and 48 h after injection, and radioactivity assessed by scintillation. Data are shown as percentage injected dose per ml blood ± standard deviation.

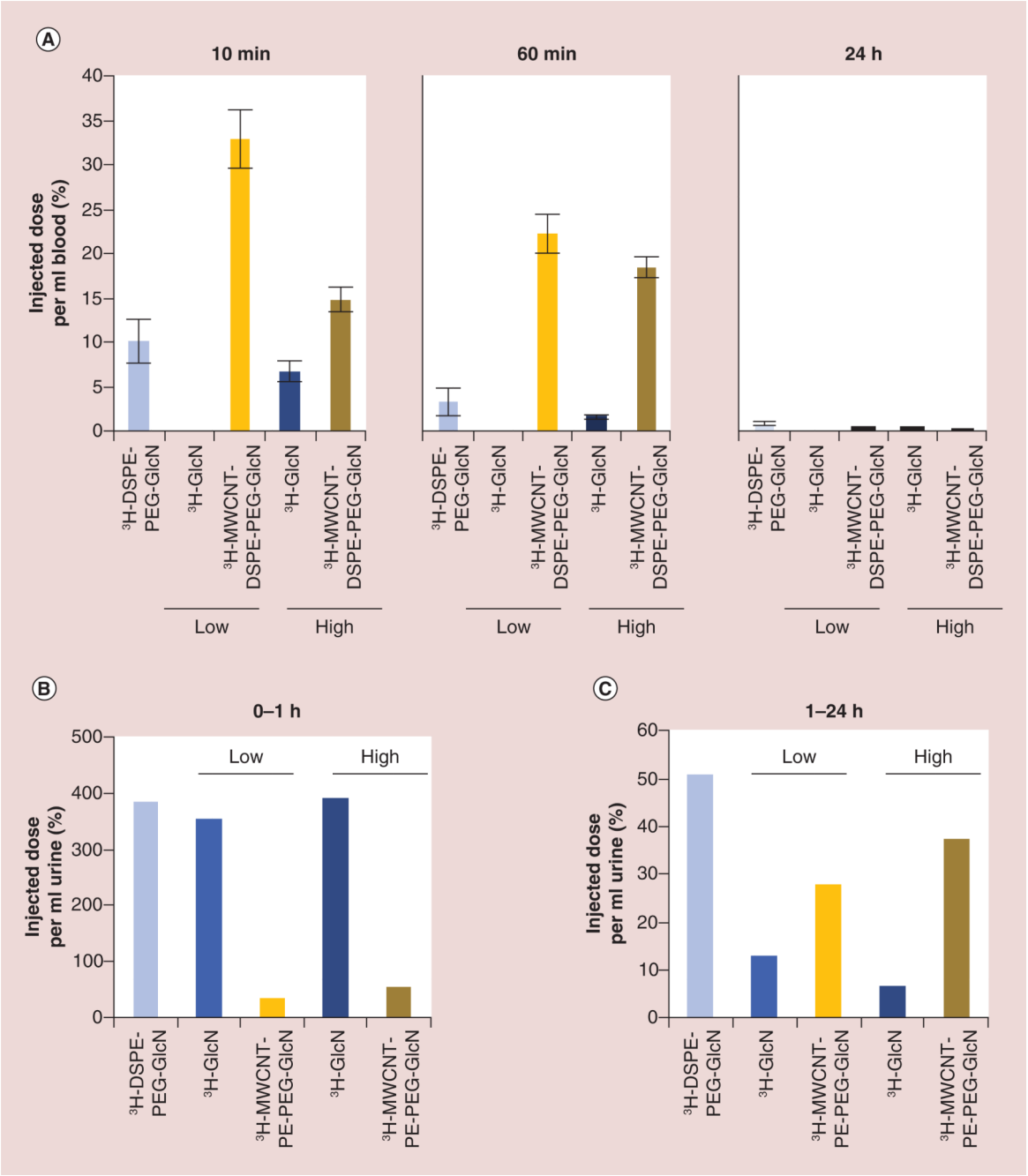

Figure 5. Blood and urinary clearance of ^{3}H-multiwalled carbon nanotube-DSPE-PEG-glucosamine

MDA-MB-231 were established as xenografts in nude mice. Nude mice (n = 3–8 per group) were injected intravenously with free ^{3}H-DSPE-PEG-GlcN, ^{3}H-GlcN (0.1 μCi [low dose] or 1.3 μCi [high dose]), ^{3}H-MWCNT-DSPE-PEG-GlcN (0.1 μCi [low dose] or 1.3 μCi [high dose] or PBS control and placed in metabolic cages. **(A)** Blood samples were obtained 10 min, 60 min and 24 h postinjection, and radioactivity was quantified by scintillation counting. Data are shown as percentage injected dose per ml blood ± standard error. **(B)** Pooled urine was collected at 0–1 h and **(C)** 1–24 h after injection, and radioactivity was

quantified by scintillation counting. Data in **(B)** are shown as percentage injected dose per ml urine.

GlcN: Glucosamine; MWCNT: Multiwalled carbon nanotube.

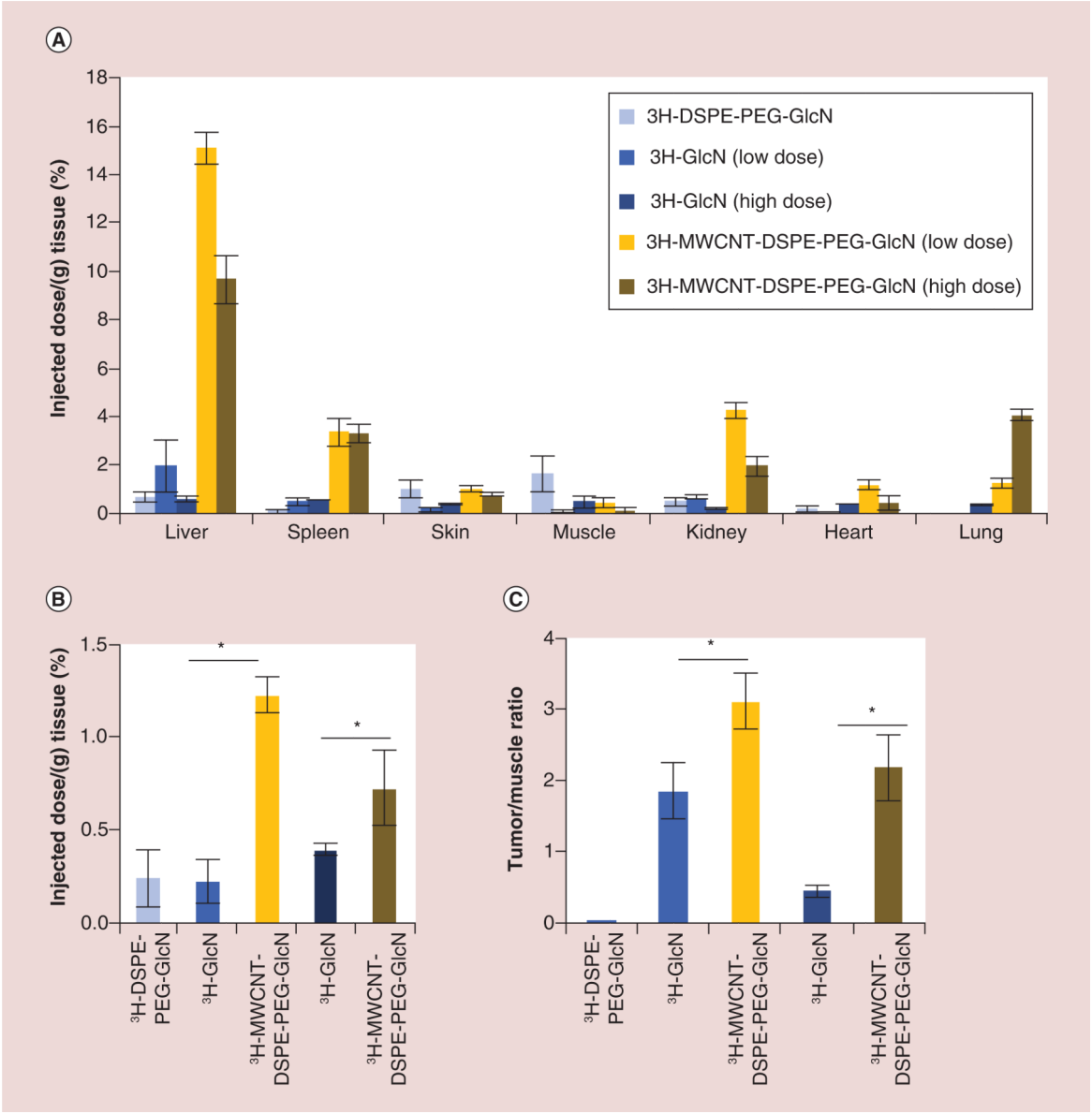

Figure 6. Tumor accumulation of ^{3}H-multiwalled carbon nanotube-DSPE-PEG-glucosamine

MDA-MB-231 were established as xenografts in nude mice. Mice (n = 3–8 per group) were injected intravenously with free ^{3}H-DSPE-PEG-GlcN (0.1 μCi), ^{3}H-GlcN (0.1 μCi [low dose] or 1.3 μCi [high dose], ^{3}H-MWCNT-DSPE-PEG-GlcN (0.1 μCi [low dose], or 1.3 μCi [high dose]), or PBS control. **(A)** 24 h after injection, tissues were excised, lysed and then radioactivity in the lysate was quantified by scintillation counting. Data are displayed as percentage injected dose per gram tissue ± standard error. **(B)** Breast cancer tumors were excised, assessed by scintillation, and data are shown as percentage injected dose per gram tumor ± standard error. **(C)** Tumor to muscle ratio is shown from tissues harvested 24 h after injection. (*$p < 0.05$, two-tailed Student's *t*-test for the indicated pairwise comparisons). GlcN: Glucosamine; MWCNT: Multiwalled carbon nanotube.